行政院國家科學委員會專題研究計畫 期中進度報告

變寬渠中強制砂洲與自由砂洲之解析與實驗研究(2/3)
期中進度報告(精簡版)

計 畫 類 別 ： 個別型
計 畫 編 號 ： NSC 95-2221-E-002-256-
執 行 期 間 ： 95 年 08 月 01 日至 96 年 07 月 31 日
執 行 單 位 ： 國立臺灣大學生物環境系統工程學系暨研究所

計 畫 主 持 人 ： 吳富春

報 告 附 件 ： 出席國際會議研究心得報告及發表論文

處 理 方 式 ： 本計畫可公開查詢

中 華 民 國 96 年 07 月 02 日

行政院國家科學委員會專題研究計畫成果報告

變寬渠中強制砂洲與自由砂洲之解析與實驗研究(2/3)

Analytical and experimental studies of forced and free bars in channels with variable width (2/3)

計畫編號：NSC 95-2211-E-002-256

執行期限：95 年 8 月 1 日至 96 年 7 月 31 日

主持人：吳富春　　國立台灣大學生物環境系統工程學系

中文摘要

本研究針對自由砂洲與強制砂洲進行非線性解析，利用奇異多尺度擾動法推導直渠道交錯砂洲之弱非線性解，並以一般擾動法推求變寬渠強制砂洲之高階非線性解。研究結果顯示自由砂洲非線性解呈現出線性解所無法獲得之天然砂洲特性。實驗結果比較顯示解析解有高估自由砂洲波數與低估砂洲高度之趨勢。強制砂洲非線性解對床形做出符合實際狀況之修正，在縱向能夠呈現次要微床形，在橫向能夠確實描述淤積斷面之床形變化，然而此種非線性效應僅在渠寬變化振幅較大時方為顯著。

關鍵詞：弱非線性解，擾動法，自由砂洲，強制砂洲。

Abstract

In this study we performed nonlinear analyses on free and forced bedforms. A singular multiple scale perturbation method is employed to derive the weakly nonlinear solution of alternate bars in straight channels, while a regular perturbation method is used for the forced bars in variable-width channels. The results reveal that the nonlinear solution of free bars exhibits natural features not captured by the linear solution. Compared to the experimental results, the analytical model tends to overestimate the wavenumber while underestimate the bar height. The nonlinear solutions of forced bars made realistic corrections to the bedforms. Longitudinally, they reveal the secondary bedform; transversely, they realistically describe the bedform where deposition occurs. However, the nonlinear effect is significant only when the amplitude of width variation is sufficiently large.

Keywords: weakly nonlinear solutions, perturbation method, free bars, forced bars.

1. Nonlinear Analysis of Free Bars in Straight Channels

A rectangular alluvial channel with width $2B_0^*$ is considered (Figure 1). The channel bed is erodible while the banks are non-erodible. The dimensionless forms of the shallow water and sediment continuity equations are:

$$U\frac{\partial U}{\partial x}+V\frac{\partial U}{\partial y}+F_0^{-2}\frac{\partial H}{\partial x}+\frac{\beta\tau_x}{D}=0 \tag{1a}$$

$$U\frac{\partial V}{\partial x}+V\frac{\partial V}{\partial y}+F_0^{-2}\frac{\partial H}{\partial y}+\frac{\beta\tau_y}{D}=0 \tag{1b}$$

$$\frac{\partial (UD)}{\partial x}+\frac{\partial (VD)}{\partial y}=0 \tag{1c}$$

$$\frac{\partial \eta}{\partial t}+Q_0\left(\frac{\partial q_x}{\partial x}+\frac{\partial q_y}{\partial y}\right)=0 \tag{1d}$$

where $t=t^*/(B_0^*/U_0^*)$; $(x,y)=(x^*,y^*)/B_0^*$; $Q_0=\dfrac{d_s^*\sqrt{Rgd_s^*}}{(1-p)D_0^*U_0^*}=$ dimensionless sediment transport parameter. No penetration boundary conditions are used for both fluid and sediment. Closure relations are given by

$$(\tau_x,\tau_y)=(U,V)(U^2+V^2)^{1/2}C_f \tag{2a}$$

$$(q_x,q_y)=(\cos\alpha,\sin\alpha)\Phi \tag{2b}$$

$$\sin\alpha=\sin\chi-\frac{r}{\beta\sqrt{\theta}}\frac{\partial\eta}{\partial y},\quad \sin\chi=\frac{V}{\sqrt{U^2+V^2}} \tag{2c-d}$$

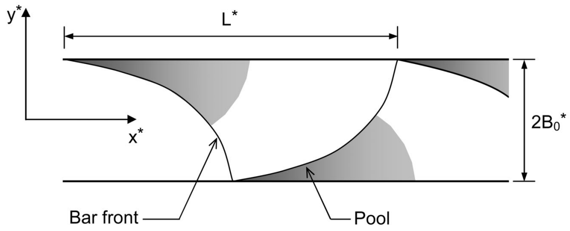

Fig 1. Definition sketch of alternate bars in a straight channel

A singular perturbation multiple scale method is employed (Colombini et al., 1987; Schielen et al., 1993). A preliminary expansion can be expressed as

$$(U,V,H,D,\eta)=(1,0,H_0,1,H_0-1)+(U',V',H',D',\eta') \quad (3a)$$

$$(\tau_x,\tau_y,q_x,q_y)=(C_{f0},0,\Phi_0,0)+(\tau_x',\tau_y',q_x',q_y') \quad (3b)$$

At the linear level, the perturbed terms are expressed by

$$(U',H',D',\eta')=Ae^{(\Omega-i\omega)t}e^{i\lambda x}\sin(\frac{\pi}{2}y)(u_1,h_1,d_1,\eta_1)+c.c.+O(A^2) \quad (4a)$$

$$V'=Ae^{(\Omega-i\omega)t}e^{i\lambda x}\cos(\frac{\pi}{2}y)v_1+c.c.+O(A^2) \quad (4b)$$

where A = amplitude of perturbation; (u_1,v_1,h_1,d_1,η_1) = complex constants; Ω and ω= bar growth rate and bar celerity; λ= dimensionless wavenumber, defined as $\lambda=\frac{2\pi}{L}$, L = dimensionless wavelength. Two parameters, Ω and ω, are obtained by the solvability condition (Nayfeh, 1981), leading to

$$\Omega-i\omega=f(\lambda,\beta,\theta_0,d_s) \quad (5)$$

which relates bar growth and bar celerity to geometric (λ), flow (β,θ_0) and sediment (d_s) parameters. The curve $\Omega=0$ separates the domain into 'stable' and 'unstable' regions, where (β_c,λ_c) are defined as the minimum value of β for bed instability and the corresponding wavenumber, respectively. Linear solutions severely suffer from the lack of precision. Spatially, they fail to describe the observed troughs and diagonal fronts. In addition, the maximum scour and deposition occur at the same cross section, which is against reality. Temporally, positive values of Ω imply continual growth of alternate bars. It is thus a matter of time before the solutions go out of control, which is the most inadequate feature of the linear solution.

$$\beta=\beta_c(1+\varepsilon),\ \lambda=\lambda_c+\varepsilon\lambda_1 \quad (6a\text{-}b)$$

where $\varepsilon \ll 1$, implying that flow conditions are in the neighborhood of the minimum instability criterion. At high orders, higher harmonics are formed due to the interaction of the lower ones. However, at some orders, the lower harmonics are reproduced. Such reappearance causes secular terms that inhibit the solutions to be valid as $t\to\infty$, thus must be suppressed. Here, the very same forms of the first harmonic are found at two orders higher, indicating a balance between $\varepsilon\frac{\partial A}{\partial T}$ and A^3, or $A\sim O(\varepsilon^{\frac{1}{2}})$. Full expansions of the perturbed terms read

$$(U',V',H',D',\eta')=\sum_{p=1}^{3}(U_p,V_p,H_p,D_p,\eta_p)(\varepsilon^{\frac{1}{2}})^p+O(\varepsilon^2) \quad (7a)$$

$$(\tau_x',\tau_y',q_x',q_y')=\sum_{p=1}^{3}(\tau_{xp},\tau_{yp},q_{xp},q_{yp})(\varepsilon^{\frac{1}{2}})^p+O(\varepsilon^2) \quad (7b)$$

At $O(\varepsilon^{\frac{1}{2}})$, the system is satisfied since (β,λ) is replaced by (β_c,λ_c), the corresponding values of (Ω,ω) are given by $(0,\omega_c)$. The amplitude A is replaced by $A(T)$. Allowing the coefficients to vary with the slow timescale T is the main feature of the multiple scale method. At $O(\varepsilon)$, the final results come to solving the non-homogeneous systems:

$$\mathbf{A}_{ij}\mathbf{X}_{ij}=\mathbf{B}_{ij} \qquad (i,j)\in\{0,2\} \quad (8)$$

At $O(\varepsilon^{3/2})$, the solutions of the variables comprise two parts. The first part is presented to counteract the secular terms; the second part represents the non-secular terms. The alternate bar height and wavelength at the equilibrium state are solved by a non-homogeneous system of equations:

$$\mathbf{A}_{31}\mathbf{X}_{31}=\mathbf{B}_{31} \quad (9)$$

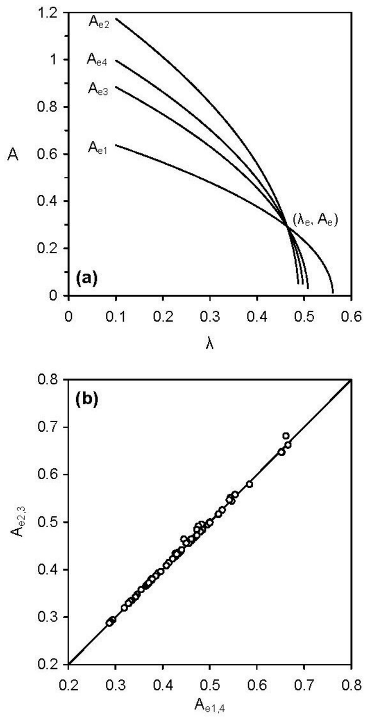

Fig 2. (a) Intersecting feature of the four solution curves for the four Landau equations; (b) Agreement between the intersection of solution curves for $A_{e2,3}$ and $A_{e1,4}$

To extend this work, define Δ_j by replacing the jth column of $\mathbf{A}_{31}$ with vector $\mathbf{B}_{31}$. To ensure the existence of the solutions $\mathbf{X}_{31}$, the solvability condition requires

$$\left|\Delta_j\right| = 0 \qquad j = 1 \sim 4 \tag{10}$$

This generates ordinary differential equations for the amplitude $A(T)$, i.e.,

$$\frac{dA}{dT} + \alpha_{1j} A + \alpha_{2j} A^2 \overline{A} = 0 \qquad j = 1 \sim 4 \tag{11}$$

which is a Landau equation. The maximum equilibrium amplitude $\left|A_{ej}\right|$ is given by

$$\left|A_{ej}\right|^2 = -\frac{\mathrm{Re}(\alpha_{1j})}{\mathrm{Re}(\alpha_{2j})} \qquad j = 1 \sim 4 \tag{12}$$

Given the flow and sediment conditions, this can be written as

$$A_{ej} = A_{ej}(\lambda_1) \qquad j = 1 \sim 4 \tag{13}$$

All individual solvability conditions must be satisfied. Hence, a solution of λ_e is sought for such that

$$A_{e1}(\lambda_e) = A_{e2}(\lambda_e) = A_{e3}(\lambda_e) = A_{e4}(\lambda_e) = A_e \tag{14}$$

The equilibrium solutions (λ_e, A_e) that answer such a relation are obtained by numerical computations. The typical intersecting feature of the four solution curves corresponding to the four Landau equations is shown in Figure 2. In Figure 3 such feature is confirmed using available experimental data on alternate bars by plotting the intersection of solution curves for $i = 2,3$ against that for $i = 1,4$. It is thus possible to predict both the wavenumber and amplitude where all necessary inputs are simple flow and sediment parameters.

2. Nonlinear Analysis of Forced Bars in Channels with Variable Width

On the problem of forced bars, time is no longer an issue. However, secular terms still do appear, only now, space-wise. In the longitudinal direction the variables alter periodically, in response to the variations of channel width. In the transverse direction, on the other hand, the validity problem exists with reappearance of the first order solutions at the third order. The geometry of the channel in question has been confined between −1 and 1. Moreover, the imposed boundary conditions guarding at two banks limit drastic deviations of the solutions. As such, a regular perturbation method would suffice to obtain solutions with an acceptable accuracy.

Using a small parameter δ for asymptotic expansion, which is given from the small amplitude of the width oscillation, $b(x)$ is expressed in a complex form:

$$b(x) = 1 + \delta b_1(x) = 1 + \delta[e^{i\lambda_b x} + c.c.] \tag{15}$$

The perturbed values can be fully expanded as

$$(U', V', H', D', \eta') = \sum_{p=1}^{2} \left(U_p, V_p, H_p, D_p, \eta_p\right)(\delta)^p + O\left(\delta^3\right) \tag{16a}$$

$$\left(\tau_x', \tau_y', q_x', q_y'\right) = \sum_{p=1}^{2} \left(\tau_{xp}, \tau_{yp}, q_{xp}, q_{yp}\right)(\delta)^p + O\left(\delta^3\right) \tag{16b}$$

Substituting these into the governing equations, boundary conditions, and closure relations, and collecting like-power terms, one obtains a linear system $O(\delta)$ and a nonlinear system $O(\delta^2)$. The variables at $O(\delta)$ are given as follows:

$$\begin{aligned}&(U_1, V_1, H_1, D_1, \eta_1)\\&= e^{i\lambda_b x}(u_1^1(y), v_1^1(y), h_1^1(y), d_1^1(y), \eta_1^1(y)) + c.c.\end{aligned} \tag{17a}$$

$$\begin{aligned}&(\tau_{x1}, \tau_{y1}, q_{x1}, q_{y1})\\&= e^{i\lambda_b x}(C_{f0}t_{x1}^1(y), C_{f0}t_{y1}^1(y),\\&\qquad \Phi_0 q_{x1}^1(y), \Phi_0 q_{y1}^1(y)) + c.c.\end{aligned} \tag{17b}$$

The superscript and subscript '1' denote $p = 1$ and the first harmonic in the longitudinal direction. The shear stresses and sediment transport rates are expressed by the flow and sediment variables. As such, the system of equations is simplified to an ODE:

$$\Gamma_0 \frac{d^4 v_1^1}{dy^4} + \Gamma_1 \frac{d^2 v_1^1}{dy^2} + \Gamma_2 v_1^1 = 0 \tag{18}$$

The boundary conditions become

$$v_1^1 = \pm i\lambda_b, \quad \frac{d^2 v_1^1}{dy^2} = \pm\Gamma_3$$

At $O(\delta^2)$, on the right hand sides of the system, interactions among variables of the lower harmonics are observed. The solutions at this order are rather tedious. The dual harmonics comprised in the first order generate many possibilities for the higher ones. The solutions can be grouped into two types, i.e., the homogeneous and particular solutions:

$$\begin{aligned}&(U_2, H_2, D_2, \eta_2, \tau_{x2}, q_{x2})\\&= e^{2i\lambda_b x}[(u_{h2}^2, h_{h2}^2, d_{h2}^2, \eta_{h2}^2, C_{f0}t_{xh2}^2, \Phi_0 q_{xh2}^2)]\\&\quad +(u_{p2}^2, h_{p2}^2, d_{p2}^2, \eta_{p2}^2, C_{f0}t_{xp2}^2, \Phi_0 q_{xp2}^2) + c.c.]\\&\quad +[(u_{h0}^2, h_{h0}^2, d_{h0}^2, \eta_{h0}^2, C_{f0}t_{xh0}^2, \Phi_0 q_{xh0}^2)\\&\quad +(u_{p0}^2, h_{p0}^2, d_{p0}^2, \eta_{p0}^2, C_{f0}t_{xp0}^2, \Phi_0 q_{xp0}^2) + c.c.]\end{aligned} \tag{19a}$$

$$\begin{aligned}(V_2, \tau_{y2}, q_{y2}) = e^{2i\lambda_b x}&[(v_{h2}^2, C_{f0}t_{yh2}^2, \Phi_0 q_{yh2}^2)\\&+(v_{p2}^2, C_{f0}t_{yp2}^2, \Phi_0 q_{yp2}^2) + c.c.]\\&+[(v_{h0}^2, C_{f0}t_{yh0}^2, \Phi_0 q_{yh0}^2)\\&+(v_{p0}^2, C_{f0}t_{yp0}^2, \Phi_0 q_{yp0}^2) + c.c.]\end{aligned} \tag{19b}$$

The superscript '2' denotes $p = 2$ and the subscripts '2' and '0' denote solutions for the 'second' and 'zero' harmonics; 'p' and 'h' in the subscript denote 'particular' and 'homogeneous' solutions. Incorporation of homogeneous solutions is required to satisfy the boundary conditions, which are main origins of the forcing effect. Grouping the terms with the same harmonics ends up solving 11 systems of equations, which can be expressed as

$$\mathbf{A}_{2j}\mathbf{X}_{2j} = \mathbf{B}_{2j} \qquad j = 1 \sim 11 \tag{20}$$

For the homogeneous solutions, the variables with a second harmonic are first solved. The second homogeneous solutions regarding the zero harmonic are then solved. From the final forms of the equations, one knows that $v_{h0}^2 = t_{yh0}^2 = q_{yh0}^2 = 0$, and $(u_{h0}^2, h_{h0}^2, d_{h0}^2, \eta_{h0}^2, t_{xh0}^2, q_{xh0}^2)$ are constants. To determine the values of these constants, two more relations are introduced. At $O(\delta^2)$, the resulting forms of these two relations are

$$\int_{-1}^{1}(U_2 + D_2 + U_1 D_1)dy = 0, \quad \int_0^{L_b}\int_{-1}^{1}\eta_2 dy dx = 0 \tag{21a-b}$$

Substituting (19a) into (21), and using the particular solutions, it is possible to solve the rest of the components in $\mathbf{X}_{h0}^2$. Thus, a complete set of solutions for $O(\delta^2)$ is obtained.

3. Results and Discussion

3.1. Nonlinear Solutions of Free Bars

The linear and nonlinear solutions of bed deformation over three wavelengths of the alternate bars are shown in Figures 3a and 3b, respectively, where the perturbed term η' is expanded to $O(\varepsilon^{\frac{1}{2}})$ for the linear solution and $O(\varepsilon)$ for the nonlinear solution. The linear result is inappropriate for describing the natural features of alternate bars because: (1) it does not show diagonal fronts and the deep pools at their downstream faces; (2) the maximum deposition and scour take place at the same cross section; and (3) the transition slope from the maximum deposition to the downstream pool is steep rather than mild. The nonlinear solution, on the other hand, exhibits such features and thus closer to the natural phenomenon.

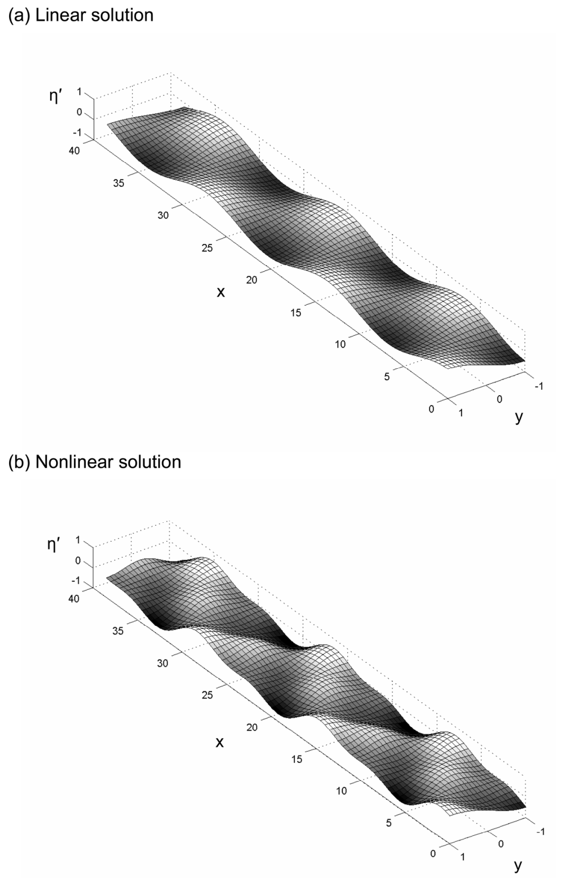

Fig. 3. (a) Linear and (b) nonlinear solutions for bed deformation of alternate bars ($\beta = 15$, $\theta_0 = 0.1$, $d_s = 0.01$)

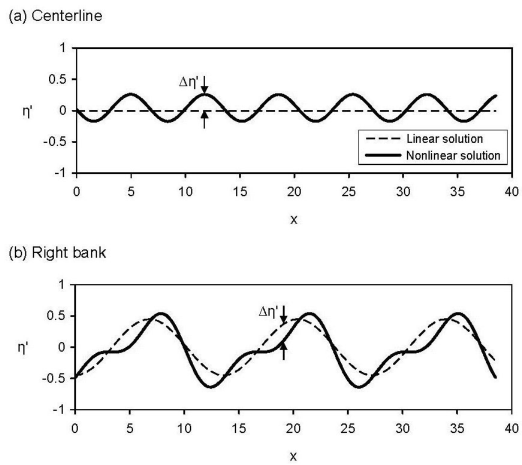

Fig. 4. Comparison of linear and nonlinear solutions of bed deformation along (a) channel centerline and (b) right bank ($\beta = 15$, $\theta_0 = 0.1$, $d_s = 0.01$)

A detailed comparison is made in Figures 4a and 4b, where the bed deformations along the centerline and right bank are shown. The difference between the two solutions is denoted by $\Delta\eta'$, which represents the effect of a pure second harmonic. Along the centerline the linear solution exhibits null variation and the nonlinear solution is fully attributed to the second harmonic. The peaks of the nonlinear solution correspond to the diagonal fronts. Along the right bank, the superposition of the two harmonics urges the bar front to shift downstream and the pool to shift upstream. This results in the milder slope from a pool to a front and steeper slope from a front to a pool.

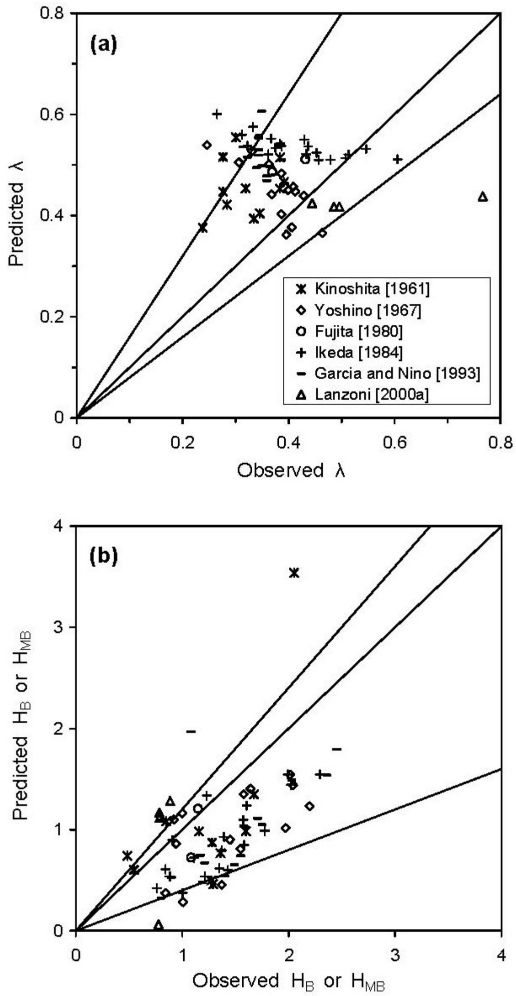

Fig. 5. Comparison between predicted and observed results of (a) bar wavenumber and (b) bar (or maximum) height

Table 1. Alternate bars wavenumber prediction errors associated with various models

Authors	Model type	Theory	Helical flow	Prediction Error
Ikeda (1984)	Empirical	Dimensional analysis	Not included	–40% ~ 80%
Blondeaux & Seminara (1985)	Analytical	Linear stability	Not included	–25% ~ 40%
Colombini et al. (1987)	Analytical	Linear stability	Not included	–30% ~ 70%
Lanzoni (2000)	Analytical	Linear stability	Included	–15% ~ 25%
This study	Analytical	Weakly nonlinear	Not included	–20% ~ 60%
Defina (2003)	Numerical	Fully nonlinear	Not included	–30%
Nelson & Smith (1989)	Numerical	Fully nonlinear	Included	4%
	Numerical	Linear theory	Not included	55%

To see whether the present model, while predicting simultaneously the bar wavelength and height, still holds a fair accuracy, the predicted results of alternate bar wavenumber and bar height are plotted against the observed results in Figures 5a and 5b, respectively. Aside from the line of perfect agreement, two other solid lines correspond to the range of error between –20% ~ 60% in Figure 5a and –60% ~ 20% in Figure 5b. A total of 66 experimental data are shown in Figure 5. In Figure 5a, more than 77% of the data fall within the –20% ~ 60% error range, indicating an overall trend of overestimation. A scatter of data with errors > 60% shows that the present model may at times overestimate the wavenumber by 3~5 times. On the other hand, for the alternate (or maximum) bar height in Figure 5b, 79% of the data fall within the –60% ~ 20% error range, indicating an overall trend of underestimation.

The wide range of prediction errors has been also reported in previous studies. In this study, such errors still exist although the range of error has been significantly reduced, especially for the prediction of bar height. A comparison of wavenumber prediction errors associated with various models is summarized in Table 1. The possible causes for these prediction errors include: (1) Misusage of shallow water equations for deep flow problems; (2) Neglecting suspended load could often over-predicts bed stability; (3) The helical flow effect is not taken into account. The alternating pattern of fronts and pools causes distortion of streamlines and thus results in the secondary flows. The importance of secondary flows in meandering channels is well known, but remains both qualitatively and quantitatively vague concerning the alternate bars in straight channels, which will be addressed in the third year.

3.2. Nonlinear Solutions of Forced Bars

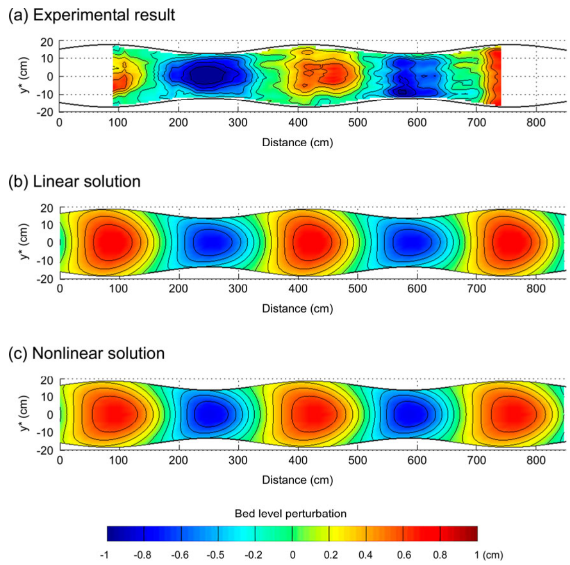

Fig. 6. Comparison between (a) experimental result, (b) linear and (c) nonlinear solutions of bed deformation in our run S6

The ability of the linear model, with the helical flow effect incorporated, in predicting various types of forced bedform has been shown in our previous work (Wu and Yeh, 2005). On this basis, we further investigate the microscopic corrections due to the nonlinear effects. The linear and nonlinear solutions for our run S6 and Bittner's run C1-11, along with the experimental results, are shown in Figures 6 and 7, respectively. In Figure 6, no apparent change is found by introducing the second-order solutions. All scour and deposition occur at very similar sections. The phase shift for the locations of the maximum deposition and scour induced by the nonlinear effects is slight. Such results are expectable since the amplitude for the channel width variation is rather small in our experiments ($\delta \approx 0.078$).

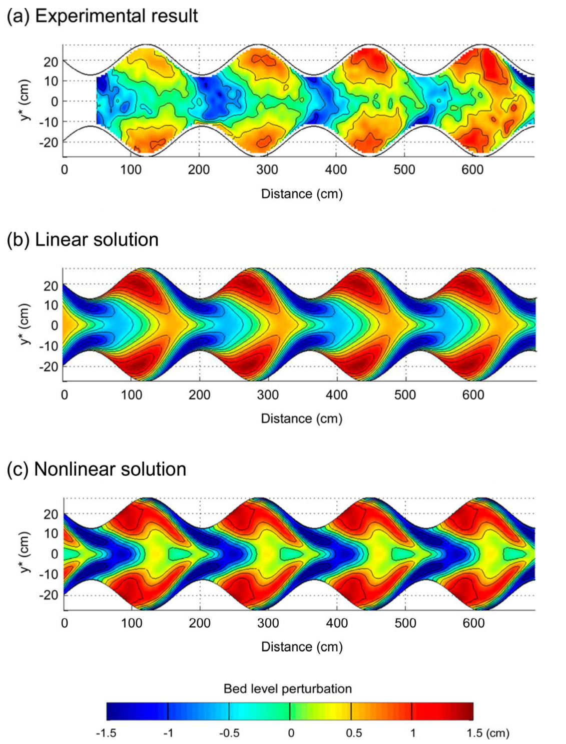

Fig. 7. Comparison between (a) experimental result, (b) linear and (c) nonlinear solutions of bed deformation in Bittner's run C1-11

For Bittner's run C1-11 where the amplitude of width variation is large ($\delta \approx 0.19$), we see in Figure 7 that the correction due to the nonlinear solutions is significant. Two major differences are observed. First, the nonlinear result is more clearly separated from the bars on the opposite side of the channel, while the linear solution predicts band-like bars with the maximum deposition at the two sides. Furthermore, the location where the bars from the two sides meet as they stretch their way to the channel centerline (referred to as the primary peak hereinafter) is also different. In Figure 7b, the bars meet at approximately halfway from the widest section to the narrowest one. In Figure 7c, the bars extended along the channel axis until they at last meet near the narrowest section. The overall bedform is better described by the nonlinear solution, especially at the centerline the linear solution tends to overestimate the bar height there. The bed deformations along the channel centerline are shown later.

Second, a secondary trough is found in the nonlinear solution, which corresponds to the second harmonic. The trough is enclosed by the side bars with a primary peak at the downstream face and another peak (referred to as the secondary peak hereinafter) at the upstream face. The peak and trough found in the linear solution are referred to as 'primary' bedforms, while those additional features revealed by the nonlinear solution are referred to as the 'secondary' bedforms. In this sense, as one travels downstream, one should encounter a secondary peak, a secondary trough, a primary peak and then a primary trough.

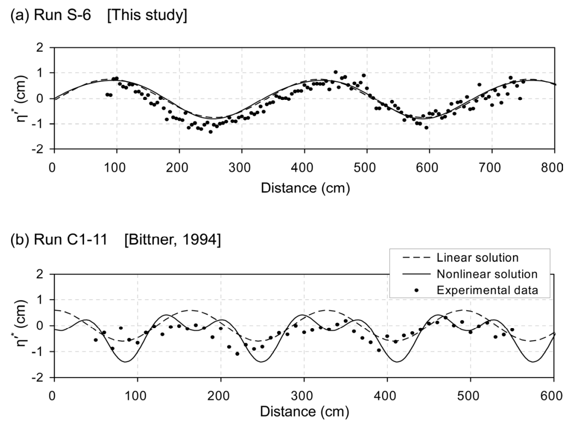

Fig. 8. Comparison of experimental and analytical results of longitudinal bed deformation profile in (a) our run S6 and (b) Bittner's run C1-11

Detailed comparisons are made in Figures 8 to 10, where the longitudinal and lateral bed deformations are shown. In Figure 8a, we see that no greater precision is obtained with additional consideration of the nonlinear effects regarding to run S6. Both linear and nonlinear solutions yield very fine agreement, both in magnitude and phase. In Figure 8b, however, a noticeable improvement is attained. The single harmonic of the linear solution tends to overestimate the bed level perturbation at the location where its maximum occurs. This is most obvious at the distance x^* = 170, 330, and 490 cm where a rise is predicted as a corresponding drop, or a secondary trough, is found. The second harmonic from solutions at $O(\delta^2)$ fairly describes such drops but underestimate the primary troughs.

For lateral profiles, both solutions agree well with the results of our run S6 (Figure 9). In the narrowest section, however, the scour depth is underestimated by ~0.6cm at the center although the general concave profile is captured. Such error could be caused by relaxing the no-slip boundary conditions, as will be discussed later. For Bittner's run C1-11 (Figure 10), the data measured over four cycles are presented with a mean value and error bars showing the range of observed values. A similar error is found in the prediction of the narrowest sections. In the narrowest sections, the deformation of the bed profiles is rather weak. An overall form of a convex can however be seen. Both linear and nonlinear solutions give the prediction of the convex form at the center but with exaggerated curvature of the convex. The maximum deviation is ~0.7cm. Hence, at the narrowest section, the scour depth is underestimated. However, this is compensated by the excessive erosion predicted at the two sides. At the widest section, on the other hand, the incorporation of the nonlinear solutions gives a positive correction toward reality. The linear solutions showed greater bar heights than the actual value, also the locations for the occurrence of the maximum bar height are shifted toward the centerline. Both defects are reduced with the nonlinear effects considered. The comparison at the narrowest sections for both experimental studies (Figures 9b and 10b) shows that the present model tends to underestimate the scour depth near the centerline but overestimate that near the bank. Such errors could arise from neglecting the no-slip boundary condition at the sidewalls whose effect becomes more important in the narrow sections (Wu and Yeh, 2005).

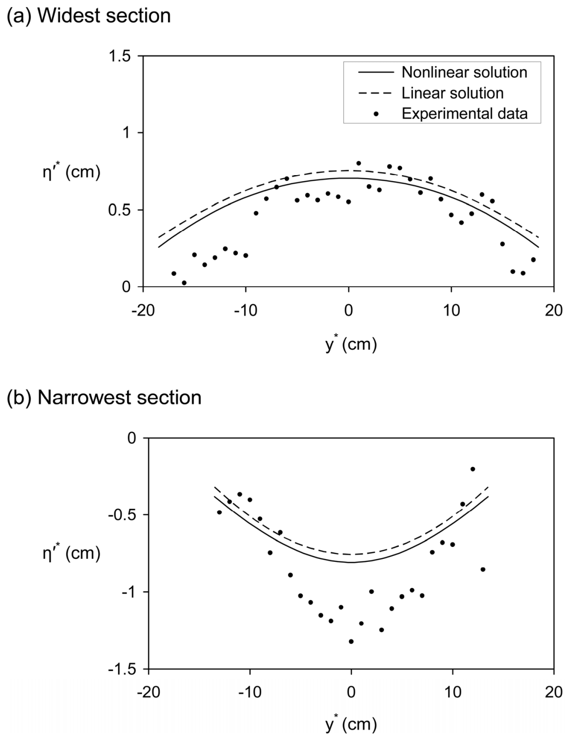

Fig. 9. Comparison of experimental and analytical results of lateral bed deformation profile in our run S6: (a) widest and (b) narrowest sections

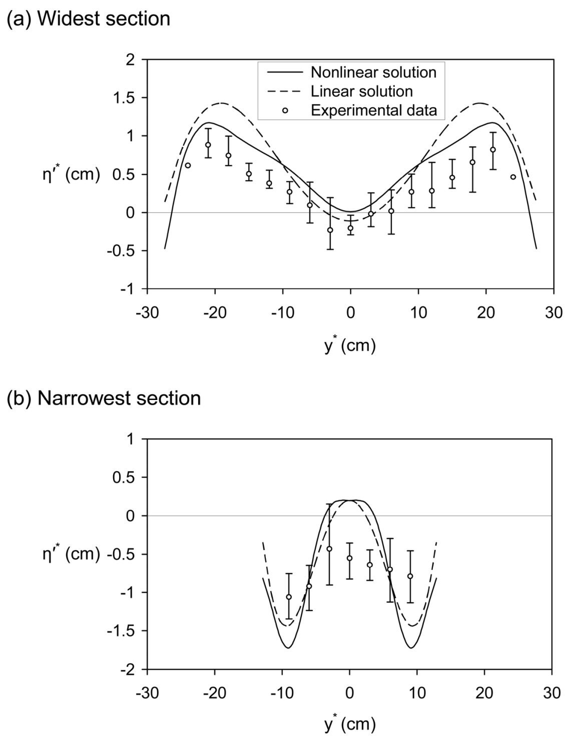

Fig. 10. Comparison of experimental and analytical results of lateral bed deformation profile in Bittner's run C1-11: (a) widest and (b) narrowest sections

4. Concluding Remarks

Nonlinear analyses are performed on the free (alternate) bars in straight channels and forced bars in variable-width channels. The results reveal that the nonlinear solution of free bars exhibits natural features not captured by the linear solution, such as diagonal fronts and downstream pools, different sections for maximum deposition and scour, and steep transition from maximum deposition to downstream pool. A comparison of the compiled experimental data and nonlinear solution further indicates that the present model tends to overestimate the wavenumber while underestimate the alternate (or maximum) bar height.

The nonlinear solutions of forced bars give realistic corrections to the bedforms in the variable-width channels. Longitudinally, they reveal the existence of the secondary bedform; transversely, they realistically describe the forced bedform when deposition occurs, although predictions at the sections where erosion occurs are less satisfactory. The nonlinear effect is, however, significant only when the amplitude of width variation is so large that the solution at $O(\delta^2)$ becomes non-negligible.

5. References

[1] Colombini, M., Seminara, G. and Tubino, M. (1987), Finite-amplitude alternate bars, *J. Fluid Mech.*, 181: 213-232.

[2] Nayfeh, A. H. (1981), *Introduction to Perturbation Techniques*, Wiley, New York, NY.

[3] Schielen, R., Doelman, A. and de Swart, H.E. (1993), On the nonlinear dynamics of free bars in straight channel, *J. Fluid Mech.*, 252: 325-356.

[4] Wu, F.-C., and T.-H. Yeh (2004), Nonlinear analysis of forced bars in variable-width channels, *Eos Trans. AGU*, *85*(28), West. Pac. Geophys. Meet. Suppl., Abstract H33A-75.

[5] Wu, F.-C., and T.-H. Yeh (2005), Forced bars induced by variations of channel width: Implications for incipient bifurcation, *J. Geophys. Res.*, *110*, F02009.

6. 計畫成果自評

本計畫擬以三年期間針對變寬渠中形成之強制砂洲與自由砂洲進行完整之線性與非線性解析，並進行水槽實驗探討其交互作用對河道平面形狀發展之影響。第二年度針對自由砂洲與強制砂洲進行非線性解析，並以水槽實驗結果驗證比較非線性解析與線性解析結果，探討非線性效應對強制與自由床形之影響。今年度研究內容與計畫書完全符合，預期目標亦全部達成。本研究利用奇異多尺度擾動法推導直渠道交錯砂洲之弱非線性解，可同時求解交錯砂洲之波數與高度，並能呈現線性解析所無法獲得之天然砂洲特性，例如交錯砂洲之對角線波前與其下游深潭、最大淤積與沖刷發生於不同橫斷面、最大淤積至下游深潭之縱向陡變等現象。本研究並以一般擾動法推求變寬渠強制砂洲之高階非線性解，對變寬渠床形做出符合實際狀況之修正，在縱向能夠呈現次要微床形，在橫向則能夠確實描述淤積斷面之床形變化，上述各種非線性效應均屬本研究之創新發現，過去相關研究中尚未有人提出，因此具有領先國際之指標性意義，而部分研究成果亦已發表於國際學術期刊與研討會。後續第三年將以前二年之研究成果為基礎，針對變寬渠中強制砂洲與自由砂洲之非線性交互作用進行更深入之探討。

出席國際學術會議心得報告

計畫編號	95-2221-E-002-256-
計畫名稱	變寬渠中強制砂洲與自由砂洲之解析與實驗研究(2/3)
出國人員姓名 服務機關及職稱	國立臺灣大學生物環境系統工程學系暨研究所 吳富春教授
會議時間地點	2007/06/04~2007/06/08
會議名稱	第一屆人工智慧與法律國際研討會
發表論文題目	A Novel HMA for Optimization of Mandatory Environmental Flows

一、參加會議經過

2007 年 6 月 4 日~8 日在美國舊金山史丹佛大學舉行之「人工智慧與法律國際研討會」(ICAIL 2007)為每兩年定期舉辦之學術性研討會，自 1987 年開始至今已有二十年歷史，本次第十一屆 ICAIL 由國際人工智慧與法律學會(IAAIL)與史丹佛大學法學院科技與法律學程共同籌辦，其目的在提升人工智慧與法律學術領域之研究與發展，並針對最新研究成果與實際應用提供與會者發表與討論之場合，藉以刺激跨領域與國際性之合作。

本次研討會開宗明義揭示人工智慧與法律學術領域之研究方向包括：

(1) 使用計算方法研究法理論辯
(2) 標準規範之正式制定
(3) 先進資訊科技應用於法律展示
(4) 應用先進資訊科技執行法律任務

而本屆研討會所規劃之重點議題包括下列 22 項：

(1) 法律知識基準系統
(2) 司法決策支援系統
(3) 概念模式基準之法律資訊修復
(4) 案例基準之法理論證
(5) 法理論辯計算模式
(6) 法律常識制定
(7) 標準規範系統制定
(8) 機器學習應用於法律
(9) 法律文書資訊自動萃取
(10) 智慧型法律教學系統
(11) 先進法律文件起草系統
(12) 不確定性證據論證
(13) 知識基準電子商務合法應用

(14) 先進網際網路法律研究工具

(15) 法律資料庫知識發掘

(16) 法律資訊修復、文件起草與知識基準系統整合

(17) 法律知識管理先進工具

(18) 線上爭議和解

(19) 電子學院標準規範模式

(20) 電子仲介契約模式

(21) 語音網路應用於法律領域

(22) 法律本體論

研討會主辦單位尤其歡迎將先進人工智慧資訊科技應用於法律執行領域之案例研究。本屆研討會共有 47 篇論文發表，分三天十四場次進行，內容涵蓋上列議題，本人所發表論文“A Novel HMA for Optimization of Mandatory Environmental Flows”即是將最新發展之直方圖吻合法(HMA)應用於強制性環境流量之優選計算，是將先進計算方法應用於執行河川環境保護政策之典型範例。

本屆研討會安排有三場專題演講，主講人分別為史丹佛大學人工智慧研究室主任 D. L. McGuinness，講題為「語音啟動計算式法律資訊系統」；史丹佛大學法學院教授 G. Fisher，講題「爭辯即講故事」；第三位學者為 IAAIL 理事長，德國柏林公開通訊系統研究所(FOKUS)資深研究員 T. F. Gordon，講題為「ICAIL 之 20 年：反映於人工智慧與法律領域」，其內容回顧過去十屆 ICAIL 之點點滴滴，並指出近二十年來，在人工智慧與法律整合領域之進步情形與未來之發展方向，對第一次參加 ICAIL 之本人而言，這場演講使本人有機會更加深入了解此一領域之過去與未來。另外，本屆研討會在第一天與最後一天安排有五場工作坊(Workshops)與兩場教學展示(Tutorials)，針對目前幾項重要議題進行互動式討論與觀摩。

二、與會心得

本次參加第十一屆 ICAIL，本人有一心得感想，即先進科技與社會法政之跨領域整合是未來必然之趨勢，過去人工智慧與法律是兩個完全不相關之領域，但透過人工智慧資訊科技與法律領域之整合，使人工智慧資訊科技之應用展示層面更為拓展，而法律領域之知識系統建置、決策支援、資訊修復、資料庫建立、標準規範制定、教育學習、文書文件起草等工作都能借助人工智慧高速計算能力，使社會法政制度之擬定與執行超脫傳統限制，達到最佳化之效果。

台灣在先進資訊科技方面有傲人之成績，但在社會法政方面卻有許多待加強改進之處，若可透過跨領域之整合，將最新觀念與現代科技引入法律領域，則受影響的不只是社會法政層面，更能擴及到受其所規範之生態環境。

A Novel HMA for Optimization of Mandatory Environmental Flows

Fu-Chun Wu
Dept of Bioenvironmental Systems Engineering
National Taiwan University, Taipei 106, Taiwan
fcwu@ntu.edu.tw

ABSTRACT

We present a novel HMA (Histogram Matching Approach) for optimization of the mandatory environmental flows. The HMA uses the degree of histogram dissimilarity as a metric for impact assessment, which is based on the quadratic-form distance between the frequency vectors of the pre- and post-impact histograms weighted by a specified similarity matrix. The HMA is coupled with an aggregated multiobjective optimization GA (genetic algorithm) and applied to a case study on the Kaoping diversion weir (Taiwan) for determining the optimal environmental flow scheme that balances the ecosystem and human needs objectives. We compare the performances of the HMA and existing RVA (Range of Variability Approach). We also employ three types of similarity function to investigate their effect on the outcomes of the HMA. The results reveal that the HMA consistently outperforms the RVA in preserving the natural flow variability regardless of what type of similarity function is used. However, no single type of similarity function can be found that would simultaneously best preserve the natural patterns of 32 IHA (Indicators of Hydrologic Alteration).

Keywords

HMA (Histogram Matching Approach); IHA (Indicators of Hydrologic Alteration); RVA (Range of Variability Approach); Mandatory environmental flows; Optimization

1. INTRODUCTION

Rivers downstream of reservoir and/or weir operation facilities typically experience a loss of natural flow variability, leading to alterations of geomorphic processes, physical habitat, nutrient cycling, water quality, temperature, and biotic interactions, thus deteriorating the health of the riverine ecosystem. In an effort to mitigate these impacts and support sustainable ecosystems, a managed release of water to meet the instream flow requirements (or termed 'environmental flows') is currently mandated by the governmental and natural resources agencies in many nations around the world.

Determining the environmental flows for the riverine ecosystems continues to be a challenge for contemporary scientists and natural resources managers. A key issue regarding the definition of environmental flows is to determine how much of the original flow regime should continue to flow down a river and onto its floodplains in order to maintain the valued features of an ecosystem. Over the last decade, the concept of 'natural flow regime' has been emerging as a paradigm for river management (Poff et al., 1997), which recognizes the full range of natural flow variability as a primary driving force for sustaining the ecological health of a river. To characterize the natural and altered flow regimes, a number of hydrologic index systems have been proposed. A thorough review can be found in Olden and Poff (2003). Richter et al. (1996) adopted 32 hydrologic parameters to develop a suite of IHA (Indicators of Hydrologic Alteration). The 32 ecologically relevant IHA are categorized by five groups of hydrologic features, i.e., flow magnitude, duration, timing, frequency, and rate of change.

The IHA have become increasingly popular tools for river management. Abundant examples can be found where researchers have employed the IHA to assess the hydrologic changes induced by flow regulations, as demonstrated by the IHA Applications Database (The Nature Conservancy, 2005). Despite the popularity of IHA, studies that incorporated the natural flow regime to optimizing water release strategies were rarely reported, primarily due to a lack of widely accepted methodology for quantifying the ecological fitness of environmental flows. Only recently, incorporation of the regime-based environmental flows in water resources and ecosystem management becomes practicable with the aid of the RVA (Range of Variability Approach) (see Shiau and Wu, 2004a, 2004b, 2006, 2007a, 2007b).

The RVA employs the natural (or pre-impact) flow series to establish the IHA target ranges (Richter et al., 1997). The management goal is to recommend environmental flow schemes that would attain the target ranges as frequently as the natural flow series. Richter et al. (1998) further suggested an IHA target range bracketed by the 25th- and 75th-percentile values, implying that 50% of the pre-impact years would have the values of the hydrologic parameter within the target range. To evaluate the deviation of

ICAIL '07 June 4-8, Palo Alto, CA USA

the post-impact flow regime from the natural conditions, Richter et al. (1998) defined a 'degree of hydrologic alteration':

$$D_{R,m} = \left| \frac{N_{o,m} - N_e}{N_e} \right| \times 100\%, \quad m = 1, \ldots, 32$$

where $D_{R,m}$ = degree of alteration for the mth IHA; $N_{o,m}$ = observed number of years whose post-impact values of the mth IHA are within the target range; N_e = expected number of years whose IHA values would fall in the target ranges = pN_T, here N_T = total number of post-impact years, p = 50% by definition. The RVA has been employed in a series of water allocation studies (Shiau and Wu, 2004a, 2004b, 2006, 2007a, 2007b) to assess the flow regime alteration induced by weir diversions and specify the optimal environmental flows balancing the ecosystem and human needs objectives.

Although the RVA is one of the first attempts to preserve the natural flow regime, it is subjected to certain potential limitations. Specifically, the RVA only concerns the frequency of a hydrologic parameter falling in the target range. Variations of the parameter value within the target range are not explicitly taken into account. Moreover, the value and frequency of the hydrologic parameter falling beyond the target range, be it above the upper- or below the lower-target, are totally ignored. These could potentially result in false evaluations of the flow regime.

We present in this work a novel HMA (Histogram Matching Approach) to resolving the issues stressed above. The HMA uses a dissimilarity metric to assess the flow regime alteration, which is based on the quadratic-form distance between the frequency vectors of the pre- and post-impact histograms weighted by a specified similarity matrix. The HMA is employed to seek the optimal environmental flow scheme for a case study on the Kaoping diversion weir, Taiwan. The performances of the HMA and RVA are compared. In addition, a sensitivity analysis is carried out on different types of similarity function.

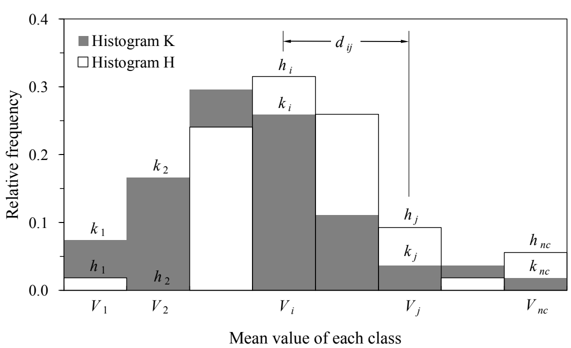

Figure 1: Schematic diagram of HMA

2. METHODS

2.1 Histogram Matching Approach (HMA)

The distribution of hydrologic data is typically expressed by a continuous probability function or a discrete histogram. The former is suitable for the situation that a sufficiently large amount of data is available for deriving an unbiased probability distribution. For most of the case where available data are limited, however, the latter is adopted by partitioning the data space into a predefined number of classes showing the frequency of occurrence in each class. The central idea behind the HMA is that two flow regimes would be similar if their frequency histograms resemble to each other. Such a resemblance is usually measured using the 'statistical distances' between the pre- and post-impact frequency histograms. As such, alteration of the flow regimes can be assessed with a distance-based dissimilarity metric.

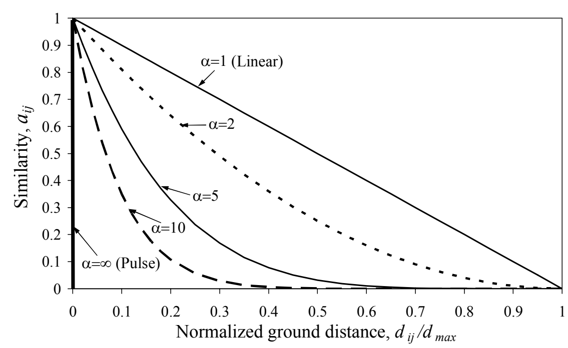

Figure 2: Similarity vs. d_{ij}/d_{max} and α

A quadratic-form distance is employed to measure the dissimilarity between two histograms H and K (Figure 1). This metric, originally proposed by Niblack et al. (1993) for color-based image retrieval, accounts for both the class-by-class correspondence and cross-class information. The quadratic-form distance d_Q is defined as

$$d_Q(H,K) = \sqrt{\left(|\mathbf{h}-\mathbf{k}|\right)^T \mathbf{A} \left(|\mathbf{h}-\mathbf{k}|\right)}$$

where $\mathbf{h} = (h_1, h_2, \ldots, h_{nc})^T$ and $\mathbf{k} = (k_1, k_2, \ldots, k_{nc})^T$ are frequency vectors of the histograms H and K; $|\mathbf{h}-\mathbf{k}|$ = statistical distance vector. The cross-class correspondence is incorporated via a similarity matrix $\mathbf{A} = [a_{ij}]$, where a_{ij} = similarity between classes i and j. The values of a_{ij} vary between 0 and 1 as a function of the ground distance between classes i and j. A general expression of a_{ij} is given by

$$a_{ij} = \left(1 - \frac{d_{ij}}{d_{\max}}\right)^{\alpha}$$

in which $d_{ij} = |V_i - V_j|$ = ground distance between classes i and j, where V_i and V_j are mean values of classes i and j; $d_{\max} = \max(d_{ij}) = |V_1 - V_{n_c}|$. Values of α are specified in a range between 1 and ∞, a linear similarity function is obtained with $\alpha = 1$, whereas a diagonal pulse similarity matrix that ignores the cross-class correspondence is obtained with $\alpha = \infty$. Variations of a_{ij} with $d_{ij}/d_{\max}$ for a variety of α are illustrated in Figure 2. As shown, the linear and pulse similarities are envelops of the similarity curve family.

2.2 Degree of Histogram Dissimilarity

To be consistent with the definition of $D_{R,m}$, the quadratic-form distance is scaled with its maximum value to define a 'degree of histogram dissimilarity':

$$D_{Q,m} = \frac{d_{Q,m}}{\max(d_{Q,m})} \times 100\%, \quad m = 1, \ldots, 32$$

where $D_{Q,m}$ = degree of histogram dissimilarity (mth IHA); $d_{Q,m}$ = quadratic-form distance (mth IHA).

2.3 Overall Degree of Flow Regime Alteration

An integrative index is used to evaluate the overall degree of flow regime alteration, i.e.,

$$D_{OQ} = \left(\frac{1}{32} \sum_{m=1}^{32} D_{Q,m}^2 \right)^{1/2}$$

where D_{OQ} = overall degree of 'hydrologic dissimilarity'. Similarly, individual values of $D_{R,m}$ is integrated as an overall degree of 'hydrologic alteration', i.e.,

$$D_{OR} = \left(\frac{1}{32} \sum_{m=1}^{32} D_{R,m}^2 \right)^{1/2}$$

Minimizing D_{OQ} or D_{OR} is regarded as equivalent to best preserving the natural flow regime, thus is taken to be a surrogate objective of the ecosystem needs in our case study.

3. CASE STUDY

3.1 Overview of Kaoping Diversion Weir

The Kaoping diversion weir is located in the midstream of Kaoping Creek, southern Taiwan. Its alluvial plain is a major agricultural area. To mitigate the impacts of groundwater overdraft and provide an alternative source of water supply, construction of the Kaoping diversion weir was initiated in 1992 and completed in 1999. The monthly flow characteristics (1951–2004) of the Lilin Bridge gauge station, located immediately above the weir site, exhibit a highly fluctuating and uneven flow pattern. The water-supply objectives of the diversion weir are to meet the agricultural and domestic water demands. Currently a minimum flow (= 9.5 m^3/s) is released from the Kaoping diversion weir for protecting the downstream water quality (WCA, 2000), which is unlikely to create a sufficient resemblance to the natural flows (Shiau and Wu, 2006). Since the post-diversion flows vary as a function of the environmental flow prescriptions, a weir operation model is used to simulate the flow series diverted for water supplies and released for ecosystem preservation.

3.2 Weir Operation Model

The system of flows in the weir operation model is depicted in Figure 3, where two flow criteria are to be met at time t, i.e., the projected diversions Q_{PD}^t and environmental flows Q_{EF}^t; Q_I^t denotes the natural (or pre-diversion) inflow; Q_{AD}^t denotes the amount of flow actually diverted for water supplies; Q_O^t denotes the post-diversion outflow. The projected monthly diversions Q_{PD}^t are summarized in Shiau and Wu (2007b), and the values of Q_{EF}^t are the only decision variable to be specified. A total of twelve Q_{EF}^t values are to be prescribed for the monthly varying environmental flow scheme. The operational rules are given by

$$\begin{cases} Q_O^t = Q_I^t, \; Q_{AD}^t = 0 & \text{if} \;\; Q_I^t \le Q_{EF}^t \\ Q_O^t = Q_{EF}^t, \;\; Q_{AD}^t = Q_I^t - Q_{EF}^t & \text{if} \;\; Q_{EF}^t < Q_I^t \le Q_{EF}^t + Q_{PD}^t \\ Q_O^t = Q_I^t - Q_{PD}^t, \;\; Q_{AD}^t = Q_{PD}^t & \text{if} \;\; Q_I^t > Q_{EF}^t + Q_{PD}^t \end{cases}$$

These operational rules are currently implemented by the Water Resources Agency of Taiwan with a constant value of Q_{EF}^t (= 9.5 m^3/s). Here we modify the operational rules by allowing the values of Q_{EF}^t to vary monthly. The daily flows at the Lilin Bridge gauge station (1951–2004) are used in the simulation as the inflow series Q_I^t. The post-diversion series, Q_O^t, are used to assess the degree of flow regime alteration. The flow series actually diverted for human demands, Q_{AD}^t, are used to evaluate the water supply deficit.

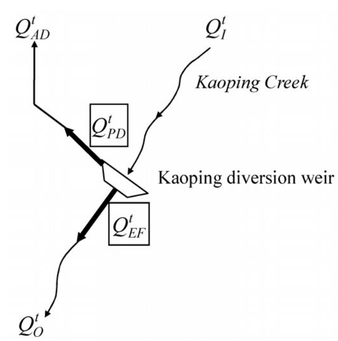

Figure 3: Flow system of Kaoping diversion weir

Table 1: Optimal sets of environmental flows Q_{EF}^{t} obtained with the RVA and HMA, the associated outcomes of D_O and SR, and statistics of D_Q and D_R

			HMA with different types of similarity function		
		RVA	Linear	Exponential (α = 5)	Pulse
D_O (%) [D_{OR} or D_{OQ}]		9.3	11.1	9.3	9.2
SR (%)		29.2	34.1	32.1	30.9
Q_{EF}^{t} (m^3/s)	January	39.7	59.0	40.4	40.5
	February	34.4	52.5	59.5	50.3
	March	27.3	66.0	28.2	30.7
	April	22.8	40.7	28.4	38.3
	May	23.4	27.5	41.0	27.6
	June	26.2	19.3	19.1	26.2
	July	9.6	14.9	13.3	26.2
	August	30.0	26.2	11.8	25.9
	September	9.6	13.3	13.3	22.0
	October	28.3	26.7	26.7	26.7
	November	47.5	65.0	48.7	21.5
	December	27.9	38.9	39.0	55.0
No. of IHA with	$D_Q \leq 5\%$	4[a] 7[b] 9[c]	10	12	14
	$5\% < D_Q \leq 10\%$	10 11 11	10	10	11
	$10\% < D_Q \leq 15\%$	7 7 7	6	7	4
	$15\% < D_Q \leq 20\%$	5 2 1	4	1	1
	$D_Q > 20\%$	6 4 4	2	2	2
No. of IHA with	$D_R \leq 33.3\%$	32	32	32	31
	$33.3\% < D_R \leq 66.7\%$	0	0	0	1
	$D_R > 66.7\%$	0	0	0	0

Superscripts a, b, and c associated with the RVA-based results denote the values of D_Q calculated with the linear, exponential, and pulse similarities, respectively.

3.3 Index of Water Supply Deficit

The shortage ratio, SR, is employed herein as an index of water supply deficit (Cancelliere et al., 1998):

$$SR = \frac{\sum_{t=1}^{N} \left| \min(Q_{AD}^{t} - Q_{PD}^{t}, 0) \right|}{\sum_{t=1}^{N} Q_{PD}^{t}} \times 100\%$$

where N = total number of days. The value of SR represents a human needs objective to be minimized with the aggregated multiobjective optimization algorithm.

3.4 Aggregated Multiobjective Optimization

The operational goal of the Kaoping diversion weir is to supply human demands while retaining the natural flow variability, which formulate a typical multiobjective optimization problem. The objective function can be expressed as

$$\text{Min}\,\{D_O, SR\}$$

where D_O = overall degree of flow regime alteration, either D_{OQ} or D_{OR} is used. Because the purpose here is to demonstrate the proposed HMA and compare the performances of HMA and RVA, rather than fully explore the tradeoffs between Pareto solutions, an aggregated multiobjective optimization genetic algorithm (AMOGA) is used to find the optimal solution of a rescaled and aggregated objective function, i.e.,

$$\text{Min}\left[\left(\frac{D_O - D_{O,\min}}{D_{O,\max} - D_{O,\min}}\right)^2 + \left(\frac{SR - SR_{\min}}{SR_{\max} - SR_{\min}}\right)^2\right]^{1/2}$$

The values of $D_{O,\max}$ and $SR_{\min}$ are obtained with an extreme condition that $Q_{EF}^{t} = 0$ at any time t, whereas $D_{O,\min}$ and $SR_{\max}$ correspond to the condition that $Q_{AD}^{t} = 0$ at any time t. The optimal set of Q_{EF}^{t} is obtained using a simple GA (Haupt and Haupt, 2004), with population size = 1000, and typical values of crossover and mutation rates = 0.8 and 0.05, respectively. The selection, crossover, and mutation operators are used to iteratively evolve a population toward the true optimal solution. The procedure is repeated until a stable optimal solution is obtained, which represents a compromise between the human and ecosystem needs objectives.

4. RESULTS AND DISCUSSION

4.1 Comparison of HMA and RVA

The results obtained with the RVA and HMA, including the optimal sets of Q_{EF}^{t}, optimal values of D_O and SR, and statistics of D_Q and D_R are summarized in Table 1, where D_{OR} and D_{OQ} correspond to the results of RVA and HMA, respectively. These values of D_O are largely on the order of 10%, indicating that the overall degrees of flow regime alteration associated with these four AMOGA-based optimal environmental flow schemes are relatively low. Although such a result may have to imply that the RVA is as useful as HMA for finding the optimal environmental flows, the strength of the HMA becomes apparent as we look at the post-optimal series of IHA. Two examples are given below to demonstrate this.

Figure 4a shows the natural and post-optimal series of monthly flows in December, obtained using both the RVA and HMA with a pulse similarity (referred to as HMA-pulse hereinafter). The post-optimal series based on the HMA-pulse closely resembles to the pattern of natural series, while the post-optimal series based on the RVA exhibits much less variability despite that 50% of the data points are within the target range. Most of these within-target data points obtained with the RVA have values that are just passing the lower target. Moreover, the percentage above the upper target is reduced to 11% while that below the lower target is increased to 39%. The frequency histograms (Figure 4b) further reveal that the post-optimal series based on the HMA-pulse closely follows the natural distribution, whereas 65% of the RVA-based post-optimal series are concentrated in the second class, which is a 37% over the corresponding natural frequency and 24% over the post-optimal frequencies resulting from both the HMA-linear and -exponential.

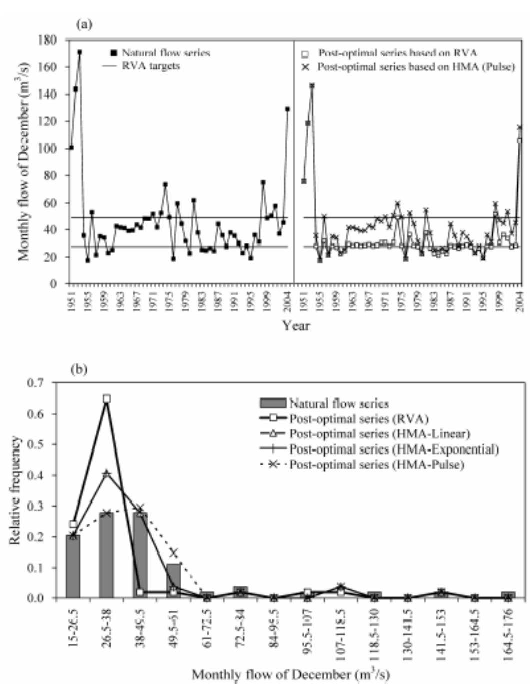

Figure 4: Monthly flows in December (a) Natural and post-optimal series; (b) Frequency histograms

As the second example, the natural and post-optimal series of annual mean low-pulse durations are shown in Figure 5a. The post-optimal series obtained with the HMA-linear exhibits a reasonably good resemblance to the natural series. The RVA-based post-optimal series of low-pulse durations is not as disturbed as that of monthly flows in December, with most of the RVA-based results being slightly greater than the corresponding values obtained with the HMA-linear. As a result, the frequency of the RVA-based post-optimal series in the fourth class is higher than the corresponding HMA-based post-optimal frequencies (Figure 5b), while the RVA-based post-optimal frequency in the first class is consistently lower than the corresponding HMA-based post-optimal frequencies.

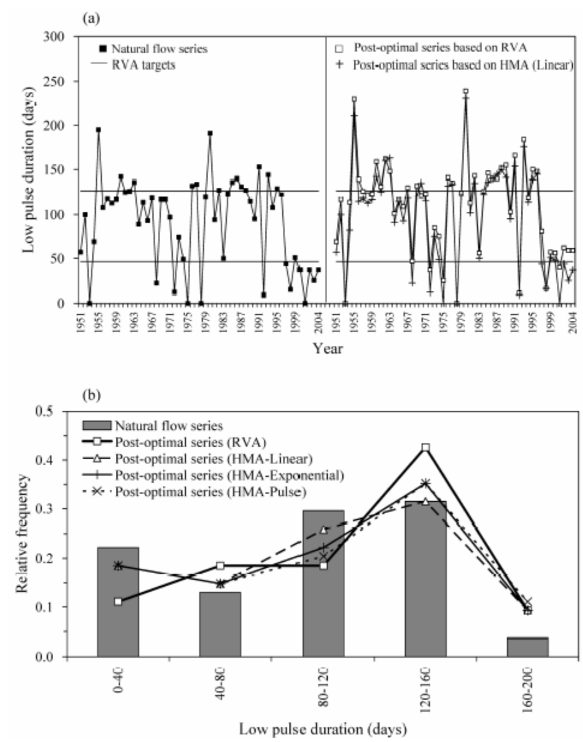

Figure 5: Mean low-pulse durations (a) Natural and post-optimal series; (b) Frequency histograms

The above two examples demonstrate that the HMA outperforms the RVA in preserving the natural flow variability, which is achieved at the cost of greater water-supply deficits, as revealed by the slightly greater values of *SR* associated with the HMA (i.e., ranging from 30.9 to 34.1%) than the RVA-based value of *SR* (= 29.2%). Such minor degradation in human needs fitness, however, may be overlooked as we compare the statistics of D_Q derived from the RVA- and HMA-based post-optimal series of 32 IHA.

Table 1 shows the numbers of IHA with the corresponding values of D_Q in five different levels, where the superscripts a, b, and c associated with the RVA-based results denote the values of D_Q calculated with the linear, exponential, and pulse similarities, respectively. Comparison of D_Q should be made between the values obtained with the same type of similarity. For $D_Q \leq 5\%$ (the most similar level), the HMA-based post-optimal numbers of IHA are consistently greater than the corresponding RVA-based values regardless of which similarity function is used, while for $D_Q > 20\%$ (the most dissimilar level), the RVA-based post-optimal numbers of IHA are consistently greater than the corresponding HMA-based values. These statistics of D_Q clearly indicate that, compared to the outcomes of the RVA, the post-optimal series of IHA obtained with the HMA preserve more of the natural flow regime via reducing the dissimilarity to the histograms of the natural series, thus offering the improved ecosystem needs fitness with only minor increases in *SR*.

4.2 Comparison of Similarity Functions

The effect of similarity function on the outcomes of HMA is explored. Three types of similarity, i.e., linear, exponential ($\alpha = 5$), and pulse, are compared. From the frequency histograms of monthly flows in December (Figure 4b), we see that the post-optimal distribution obtained with the HMA-pulse is most similar to the natural pattern, while the identical results obtained with the linear and exponential similarities are inferior. The best outcome associated with the HMA-pulse is attributed to the largest value of Q_{EF}^t prescribed (Table 1), which, however, does not necessarily mean that the environmental flows prescribed with the HMA-pulse are greater than those obtained with other types of similarity function. For example, the value of Q_{EF}^t prescribed for November using the pulse similarity is smallest, resulting in the only value of D_R ranging between 33.3% and 66.7% while others are below 33.3% (Table 1). The frequency histograms of the low pulse durations (Figure 5b), on the other hand, reveal that the post-optimal histogram associated with the HMA-linear is most similar to the natural pattern, whereas that associated with the HMA-pulse is least similar to the natural one. These data provide information from which a general conclusion can be drawn. Specifically, there is no single type of similarity function that would make the post-optimal series of 32 IHA simultaneously best retain the natural flow regime. Nevertheless, practical guidelines may be obtained from the finding of this work. For the situations where water-supply reliability is of critical concern, the pulse similarity is recommended because it would assure the smallest water-supply deficit. However, if minor degradation in the water-supply reliability may be overlooked, the linear similarity is suggested because it would generally result in the post-impact flows that most satisfactorily resemble to the natural flow regime.

5. CONCLUSIONS

Herein a novel HMA for assessment of flow regime alteration is presented. The proposed HMA is applied to a case study on the Kaoping diversion weir for determining the optimal mandatory environmental flows. The results reveal that the HMA eliminates the shortcoming of the existing RVA, thus consistently outperforms in preserving the natural flow variability regardless of which similarity function is used. Such performances of the HMA are achieved via reducing the dissimilarities to the pre-impact frequency histograms of 32 IHA. However, no single type of similarity function can be found that would simultaneously best retain the natural patterns of 32 IHA. Selection of an appropriate similarity function may be based on the finding of this work.

6. REFERENCES

Cancelliere A, Ancarani A, Rossi G. 1998. Susceptibility of water supply reservoirs to drought conditions. *J. Hydrol. Eng.* **3**: 140-148.

Haupt RL, Haupt SE. 2004. *Practical Genetic Algorithms*. John Wiley: Hoboken, NJ.

Niblack W, Barber R, Equitz W, Flickner MD, Glasman EH, Petkovic D, Yanker P, Faloutsos C, Taubin G, Heights Y. 1993. Querying images by content, using color texture, and shape. In *SPIE Conference on Storage and Retrieval for Image and Video Databases* **1908**: 173-187.

Olden JD, Poff NL. 2003. Redundancy and the choice of hydrologic indices for characterizing streamflow regimes. *River Res. Appl.* **19**: 101-121.

Poff NL, Allan JD, Bain MB, Karr JR, Prestegaard BD, Richter BD, Sparks RE, Stromberg JC. 1997. The natural flow regime: A paradigm for river conservation and restoration. *Bioscience* **47**: 769-784.

Richter BD, Baumgartner JV, Powell J, Braun DP. 1996. A method for assessing hydrologic alteration within ecosystems. *Cons. Biology* **10**: 1163-1174.

Richter BD, Baumgartner JV, Wigington R, Braun DP. 1997. How much water does a river need. *Freshwater Biology* **37**: 231-249.

Richter BD, Baumgartner JV, Braun DP, Powell J. 1998. A spatial assessment of hydrologic alteration within a river network. *Regulated Rivers: Research and Management* **14**: 329-340.

Shiau JT, Wu FC. 2004a. Assessment of hydrologic alterations caused by Chi-Chi diversion weir in Chou-Shui Creek, Taiwan: Opportunities for restoring natural flow conditions. *River Research and Applications* **20**: 401-412.

Shiau JT, Wu FC. 2004b. Feasible diversion and instream flow release using Range of Variability Approach. *Journal of Water Resources Planning and Management* **130**: 395-404.

Shiau JT, Wu FC. 2006. Compromise programming methodology for determining instream flow under multiobjective water allocation criteria. *Journal of the American Water Res. Assoc.* **42**: 1179-1191.

Shiau JT, Wu FC. 2007a. A dynamic corridor-searching algorithm to seek time-varying instream flow releases for optimal weir operation: Comparing three indices of overall hydrologic alteration. *River Research and Applications* **23**: 35-53.

Shiau JT, Wu FC. 2007b. Pareto-optimal solutions for environmental flow schemes incorporating the intra- and inter-annual variability of the natural flow regime. *Water Resources Research* **43**: (in press).

The Nature Conservancy. 2005. *IHA Applications Database*. http://www.nature.org/initiatives/freshwater/files/iha_apps.pdf

Water Conservancy Agency (WCA). 2000. *Feasibility Planning on Conjunctive Use of Tsengwen Reservoir and Nanhua Reservoir*. WCA: Taichung, Taiwan (in Chinese).